

# Altered axonal targeting and short-term plasticity in the hippocampus of *Disc1* mutant mice

Mirna Kvjajo<sup>a,b,1</sup>, Heather McKellar<sup>c,1</sup>, Liam J. Drew<sup>b</sup>, Aude-Marie Lepagnol-Bestel<sup>b,2</sup>, Lan Xiao<sup>d,e</sup>, Rebecca J. Levy<sup>f</sup>, Richard Blazeski<sup>g</sup>, P. Alexander Arguello<sup>f</sup>, Clay O. Lacefield<sup>f</sup>, Carol A. Mason<sup>g</sup>, Michel Simonneau<sup>h</sup>, James M. O'Donnell<sup>d,e</sup>, Amy B. MacDermott<sup>b,f</sup>, Maria Karayiorgou<sup>a,i,3</sup>, and Joseph A. Gogos<sup>b,f,3</sup>

<sup>a</sup>Department of Psychiatry, Columbia University Medical Center, New York, NY 10032; <sup>b</sup>Department of Physiology and Cellular Biophysics, Columbia University Medical Center, New York, NY 10032; <sup>c</sup>Integrated Program in Cellular, Molecular, and Biophysical Studies, Columbia University, New York, NY 10032; <sup>d</sup>Department of Behavioral Medicine and Psychiatry, West Virginia University Health Sciences Center, Morgantown, WV 26505-2854; <sup>e</sup>Department of Neurobiology and Anatomy, West Virginia University Health Sciences Center, Morgantown, WV 26506; <sup>f</sup>Department of Neuroscience, Columbia University Medical Center, New York, NY 10032; <sup>g</sup>Department of Pathology, College of Physicians and Surgeons, Columbia University, New York, NY 10032; <sup>h</sup>Institut National de la Santé et de la Recherche Médicale U675, Institut Fédératif de Recherche 02, Faculté de Médecine Xavier Bichat, Université Paris Diderot-Paris 7, 75018 Paris, France; and <sup>i</sup>Division of Psychiatric Genetics, New York State Psychiatric Institute, New York, NY 10032

Edited\* by Gerald D. Fischbach, The Simons Foundation, New York, NY, and approved October 7, 2011 (received for review September 1, 2011)

**Carefully designed animal models of genetic risk factors are likely to aid our understanding of the pathogenesis of schizophrenia. Here, we study a mouse strain with a truncating lesion in the endogenous *Disc1* ortholog designed to model the effects of a schizophrenia-predisposing mutation and offer a detailed account of the consequences that this mutation has on the development and function of a hippocampal circuit. We uncover widespread and cumulative cytoarchitectural alterations in the dentate gyrus during neonatal and adult neurogenesis, which include errors in axonal targeting and are accompanied by changes in short-term plasticity at the mossy fiber/CA3 circuit. We also provide evidence that cAMP levels are elevated as a result of the *Disc1* mutation, leading to altered axonal targeting and dendritic growth. The identified structural alterations are, for the most part, not consistent with the growth-promoting and premature maturation effects inferred from previous RNAi-based *Disc1* knockdown. Our results provide support to the notion that modest disturbances of neuronal connectivity and accompanying deficits in short-term synaptic dynamics is a general feature of schizophrenia-predisposing mutations.**

psychiatric disease | rare mutation | mouse model

The schizophrenia (SCHZ) susceptibility gene *DISC1* was identified through a balanced chromosomal translocation (1;11)(q42.1;q14.3) segregating with SCHZ and mood disorders in a large Scottish pedigree. This is the only confirmed disease risk allele within the *DISC1* locus. The biology of *DISC1* is being interrogated with a variety of approaches, such as acute RNAi-mediated gene knockdown (1–4), overexpression of truncated forms of the human *DISC1* (5, 6), and chemical mutagenesis (7). Although they provide information about potential pathways related to *DISC1*, these approaches are not meant to recapitulate the integrated effects of the pathogenic translocation, and the relevance of these findings to SCHZ pathogenesis remains uncertain.

We used a disease-focused knockin approach to introduce a truncating lesion in the endogenous murine *Disc1* ortholog designed to model the effects of the (1;11) translocation (Mouse Genome Informatics nomenclature *Disc1*<sup>Tm1Kara</sup>) (8, 9). Although the divergence in the human and mouse *Disc1* gene does not allow an exact replication of the human translocation, this mouse model approximates very closely the Scottish mutation. One advantage of our approach is that it retains endogenous levels as well as spatial and temporal patterns of *Disc1* expression, and it preserves short N-terminal isoforms that are presumably unaffected by the Scottish translocation and seem to be expressed at relatively higher levels in the hippocampus (HPC) of patients with SCHZ (10). A comprehensive behavioral analysis has shown that *Disc1*<sup>Tm1Kara</sup> mice display a unique profile of cognitive impairments, including specific and robust deficiencies in working memory (WM) tests

(8, 9), which may relate to similar cognitive deficits prominent in psychotic disorders.

*DISC1* is widely expressed during embryonic and early postnatal development, with high expression persisting in the adult HPC and especially, the dentate gyrus (DG) (11). Abnormal neuronal development and function of the DG has been proposed as a risk factor for a number of psychiatric disorders, including depression and SCHZ (12), and thus, it could contribute to the increased rates of SCHZ and mood disorders found in the Scottish pedigree. Neuropathological studies of patients with SCHZ have found a number of variable and modest cytoarchitectural disturbances in the DG-CA3 regions, including impaired dendritic arborization (13, 14), as well as alterations in synaptic density and mossy fibers (MFs) terminal structure (12). DG receives, as a primary input, sensory information from the entorhinal cortex and projects exclusively to the CA3 region of the HPC, acting as an important processor of sensory input for integration in hippocampal networks. The output of the DG, the MFs, is characterized by precise topography and remarkable activity-dependent short-term synaptic plasticity (STP) and plays a critical role in regulating activity in its target CA3 area. There is considerable evidence that variation in axonal cytoarchitecture and alterations in neural activity and synaptic plasticity in DG may affect cognition (15, 16), including performance in some spatial WM tasks (17, 18) similar to the ones impaired by *Disc1*<sup>Tm1Kara</sup>. Disrupting synaptic plasticity within the DG also impairs performance on spatial WM paradigms (19).

Using our mouse model, here, we uncover widespread cytoarchitectural alterations in the DG granule cells (GCs) both early in neonatal development and in the adult brain, including previously unsuspected errors in axon pathfinding. We also show that deficits in neural architecture are accompanied by altered excitability as well as impaired STP at MF synapses. Finally, we provide evidence that cAMP levels are elevated because of the *Disc1* mutation and modulate axonal pathfinding and dendritic growth of hippocampal neurons by altering expression of axon guidance molecules and local cAMP signaling at the growth cone. Our work

Author contributions: M. Kvjajo, H.M., L.J.D., A.-M.L.-B., C.A.M., M.S., J.M.O., A.B.M., M. Karayiorgou, and J.A.G. designed research; M. Kvjajo, H.M., L.J.D., A.-M.L.-B., L.X., R.J.L., R.B., P.A.A., and C.O.L. performed research; C.O.L. contributed new reagents; M. Kvjajo, H.M., L.J.D., A.-M.L.-B., L.X., and R.J.L. analyzed data; and M. Kvjajo, H.M., L.J.D., M. Karayiorgou, and J.A.G. wrote the paper.

The authors declare no conflict of interest.

\*This Direct Submission article had a prearranged editor.

<sup>1</sup>M.Kvjajo and H.M. contributed equally to this work.

<sup>2</sup>Present address: Laboratoire de Génomique Fonctionnelle, Commissariat à l'Energie Atomique, 91057 Evry, France.

<sup>3</sup>To whom correspondence may be addressed. E-mail: jag90@columbia.edu or mk2758@columbia.edu.

See Author Summary on page 19471.

This article contains supporting information online at [www.pnas.org/lookup/suppl/doi:10.1073/pnas.1114113108/-DCSupplemental](http://www.pnas.org/lookup/suppl/doi:10.1073/pnas.1114113108/-DCSupplemental).

offers a clear and detailed account of the effect of an SCHZ risk mutation on the development, structure, and synaptic properties of HPC circuits.

## Results

***Disc1<sup>Tm1Kara</sup>* Impairs Development of Neonatally Born GCs.** The DG is formed by two distinct populations of GCs: neonatally born neurons that are generated during the first 2 postnatal wk (neonatal neurogenesis) representing the majority of GCs (20), and adult-born neurons that populate the mature DG through continuous neurogenesis (21). Previous analysis in mice carrying the *Disc1<sup>Tm1Kara</sup>* mutation showed decreased numbers of proliferating cells and immature adult-born neurons (9). To assess whether *Disc1<sup>Tm1Kara</sup>* affects neonatal neurogenesis, mice were injected with BrdU at postnatal day (P)10 to label proliferating cells and killed at P11. Evaluation of BrdU incorporation revealed a significant decrease in the number of labeled cells in mutant mice ( $P = 0.037$ ) (Fig. 1A and B), indicating that *Disc1<sup>Tm1Kara</sup>* affects neurogenesis in the developing DG similarly to the adult DG (9).

P11 *Disc1<sup>Tm1Kara</sup>* mice carrying one *Thy1-GFP* reporter allele were used to analyze the dendritic morphology of GCs. GFP-positive cells generated during this period were predominantly confined to the outer layer of the DG and displayed a morphology characterized by multiple primary dendrites. Analysis of their complexity revealed a decrease in the number of dendritic segments ( $P = 0.016$ ) (Fig. 1C and D) and branching points ( $P = 0.017$ ) (Fig. S14). This result suggests that the decrease in dendritic arborization observed in adult *Disc1<sup>Tm1Kara</sup>* mice (9) may stem from changes in early development.

We characterized the MF of P11 GCs using calbindin immunohistochemistry. In wild-type (WT) mice, MFs accumulate in the DG hilus and then, project to the CA3 pyramidal cell layer segregated in two distinct bundles: the large suprapyramidal bundle (SPB) that travels adjacent to and above the pyramidal layer and a smaller infrapyramidal bundle (IPB) that travels below the pyramidal layer, with sparse fibers connecting the IPB and SPB (22). In mutant mice, there was a prominent increase in fibers crossing the pyramidal cell layer, causing the IPB and SPB to fail to clearly segregate into the two distinct tracts until they were significantly

farther away from the hilus than in the WT mice (Fig. 1E). Quantitative determination of the point at which the SPB and IPB separated revealed that, although WT fibers typically segregated on average 50  $\mu\text{m}$  away from the hilus, mutant fibers only segregated at a distance of  $\sim 200 \mu\text{m}$  ( $P = 0.0002$ ) (Fig. 1F). In addition, the total length of both bundles was slightly ( $\sim 6\text{--}7\%$ ) increased (SPB:  $P = 0.018$ ; IPB:  $P = 0.022$ ) (Fig. S1B and C). Inspection of hippocampal morphology on Nissl-stained sections showed that, as in adult mice (8, 9), lamination of CA3 neurons was preserved (Fig. S1D), suggesting that the abnormal lamination of MFs does not stem from altered positioning of their target cells. Analysis in adult *Disc1<sup>Tm1Kara</sup>* mice revealed that, although alterations in axonal patterning could be still observed (Fig. S1E), there was no overall significant change in the location of SPB and IPB separation ( $P = 0.37$ ) (Fig. S1F). The length of SPB ( $P = 0.033$ ) but not IPB ( $P = 0.55$ ) remained slightly ( $\sim 5\%$ ) increased (Fig. S1G and H).

## *Disc1<sup>Tm1Kara</sup>* Results in Altered Laminar Distribution of MF Terminals.

When MFs exit the hilar region and reach the pyramidal cell layer, the SPB makes synaptic contacts with the apical dendrites, whereas the IPB synapses with the basal dendrites (22). To determine whether altered axonal targeting also affected the laminar distribution of MF terminals (MFT), we stained for the presynaptic marker synaptophysin. Notably, our analysis revealed ectopic MFTs invading the pyramidal layer in the proximal and distal CA3 of P11 mice (Fig. 2A and B).

We next exploited the low-expression levels of *Thy1-GFP* at P11 to visualize and quantify the laminar distribution of individual GFP-labeled MFT. We analyzed the distribution of terminals above (belonging to the SPB), below (belonging to the IPB), and within the pyramidal cell layer in both the proximal and distal CA3 (Fig. 2C and D and Fig. S2A and B). In all three genotypes, the SPB and IPB terminals partially overlapped with the pyramidal cell layer. However, quantification in the proximal CA3 in mutant mice showed an  $\sim 25\%$  increase in the portion of synaptic terminals located within this layer at the expense of terminals localized to the SPB ( $P < 0.0001$ ) or IPB ( $P < 0.0002$ ) (Fig. 2E). A quantification in the distal CA3 revealed an  $\sim 10\%$  increase in the portion of terminals located within the pyramidal cell layer in

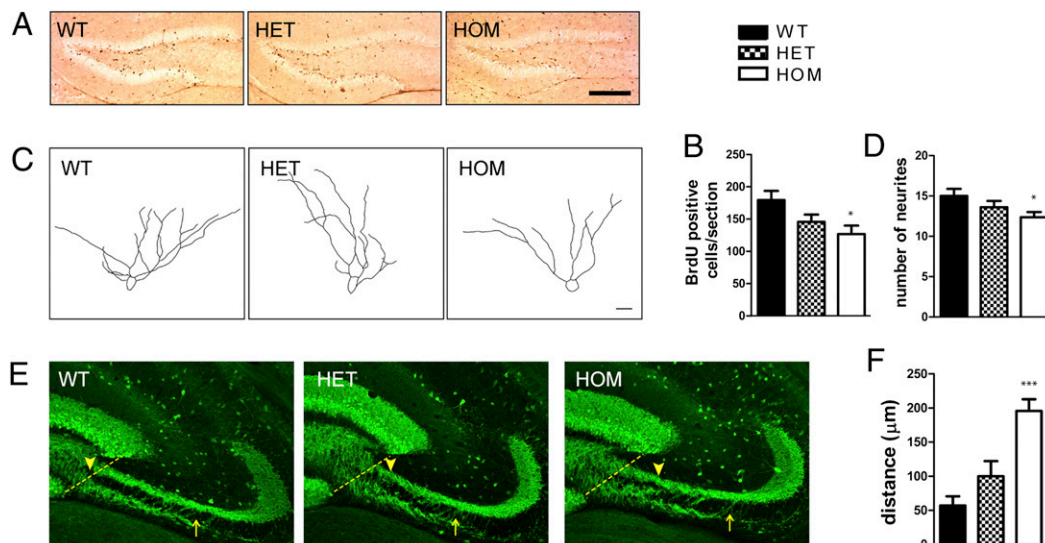


**Fig. 1.** Proliferation, dendritic complexity, and axonal projections in the developing DG. (A and B) BrdU labeling in the P11 DG (A) shows a decrease in the number of proliferating cells in mutant mice (B;  $P = 0.037$ ;  $n = 6, 6,$  and  $5$  mice). (C and D) Representative tracings of GC in the P11 DG (C) and quantification (D) showing decreased numbers of dendritic segments/neuron ( $P = 0.016$ ;  $n = 26, 28,$  and  $28$  cells). (E and F) MF projections in P11 mice. (E) Fibers connecting the IPB and SPB are increased in mutant mice, altering the separation of IPB and SPB. The dotted line represents the reference point from which the measurement of the distance at which IPB and SPB separate was initiated. Arrowheads indicate points of IPB and SPB separation in the three genotypes. Arrows represent the endpoint of the measurement. (F) Quantification (in micrometers) of the point of separation, showing decreased segregation of mutant fibers ( $P = 0.0002$ ;  $n = 6$  mice/genotype). Values represent mean  $\pm$  SEM. \* $P < 0.05$ ; \*\*\* $P < 0.0005$ . (Scale bars: A,  $200 \mu\text{m}$ ; C,  $20 \mu\text{m}$ ; E,  $100 \mu\text{m}$ .)

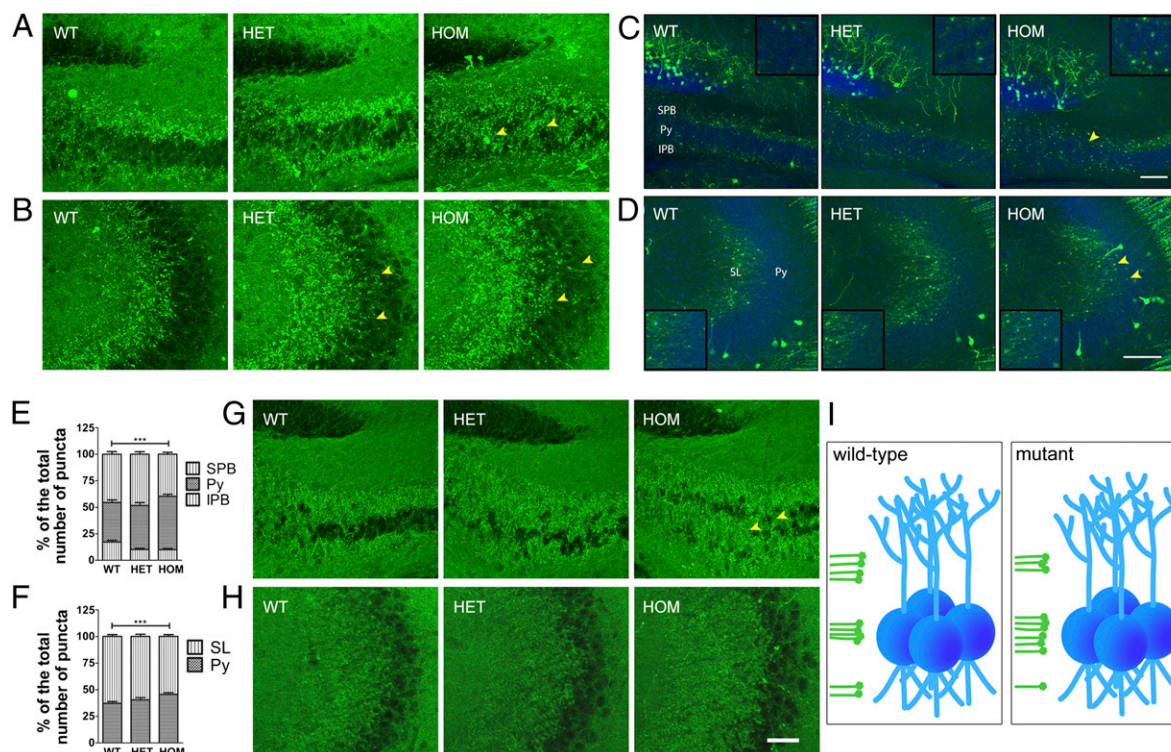


**Fig. 2.** Analysis of MFT laminar distribution. (A and B) Synaptophysin immunoreactivity in P11 proximal (A) and distal (B) MFs. Ectopic terminals are labeled with arrowheads. (C–F) MF terminal distribution in the proximal (C) and distal (D) CA3 region in P11 *Disc1<sup>Tm1Kara</sup>/Thy1-GFP* mice. MFTs are visible as green puncta. The pyramidal cell layer (Py) is in blue. Arrowheads indicate altered distribution of MFT. Insets show MFT puncta in the Py. (E) In the proximal CA3, more terminals (in percentages) are found in the Py of HOM mice at the expense of terminals located in the SPB ( $P < 0.0001$ ) and IPB ( $P < 0.0002$ ). (F) Quantification in the distal CA3 revealed more terminals (in percentages) in the Py of HOM mice ( $P = 0.005$ ) at the expense of those terminals located in the stratum lucidum (SL;  $P < 0.0001$ ;  $n = 4, 4,$  and  $5$  mice). (G and H) Synaptophysin immunoreactivity in adult proximal (G) and distal (H) MFs. Ectopic terminals are labeled with arrowheads. (I) A schematic representation of MF projections (green) in the proximal CA3 and their interaction with pyramidal neurons (blue). Values represent mean  $\pm$  SEM. \*\*\* $P < 0.0005$ . (Scale bars: A, B, G, and H (shown in H), 50  $\mu$ m; C and D, 100  $\mu$ m.) IPB, infrapyramidal bundle; Py, stratum pyramidale; SL, stratum lucidum; SPB, suprapyramidal bundle.

*Disc1<sup>Tm1Kara</sup>* mice ( $P = 0.005$ ) at the expense of terminals located in the stratum lucidum ( $P < 0.0001$ ) (Fig. 2F). Consistent with the pattern of axonal lamination, synaptophysin staining revealed that changes in MFT distribution were considerably attenuated in adult mice. Ectopic terminals could be still observed in the proximal but not distal CA3 (Fig. 2G and H). Overall, our results show that *Disc1<sup>Tm1Kara</sup>* alters the lamina-specific projections of MF (Fig. 2I).

***Disc1<sup>Tm1Kara</sup>* Impairs Development of DG Adult-Born Neurons.** To investigate if *Disc1<sup>Tm1Kara</sup>* affects the development of adult-born neurons, we performed a comprehensive analysis of their maturation using a retroviral labeling strategy that allows specific labeling of dividing progenitor cells in vivo. Adult *Disc1<sup>Tm1Kara</sup>* mice were stereotaxically injected with an oncovirus expressing GFP only in dividing cells, and adult-born neurons were analyzed at 1, 2, and 4 wk after the injection (Fig. 3A). Recent reports showed that shRNA-mediated knockdown of *Disc1* in individual adult-born neurons resulted in accelerated maturation manifested as a dramatic increase in dendritic complexity, spine density, and cell soma size (2) as well as a marked increase in axonal length (3). Analysis of 1- and 2-wk-old neurons revealed no differences among genotypes in the number of dendritic segments, although a trend for increased dendritic complexity was observed at 2 wk postinjection (Fig. 3B and C) [1 wk postinjection (wpi):  $P = 0.4$ ; 2 wpi:  $P = 0.319$ ]. However, at 4 wpi, homozygous (HOM) and heterozygous (HET) *Disc1<sup>Tm1Kara</sup>* neurons had significantly decreased numbers of dendritic segments ( $P = 0.02$ ) (Fig. 3D) and branch points ( $P = 0.015$ ) (Fig. S3A). These results suggest that there may be a distinct developmental trajectory in mutant neurons with an increase in the rate of dendritic outgrowth at early developmental

stages of the neurons and a subsequent decrease in mature adult-born neurons.

Soma size was not different at 1 wpi. At 2 wk, there was an  $\sim 10\%$  increase in HET and HOM neurons ( $P = 0.047$ ), which at 4 wk, persisted only in HET mice ( $P = 0.015$ ) (Fig. S3B–D), suggesting potential compensatory effects in HOM mice. The implications of these findings on the rate of neuronal maturation are unclear. It should be noted, however, that we did not observe any premature formation of spines at 1 and 2 wk or changes in spine density at 4 wk on either proximal ( $P = 0.34$ ) or distal dendrites ( $P = 0.5$ ) (Fig. S3E–G). Finally, we did not observe any alteration in axonal length in *Disc1<sup>Tm1Kara</sup>* mice 2 wpi when the axons left the DG hilus (Fig. S3H and I) ( $P = 0.27$ ). At 4 wk, when the labeled axons had fully invaded CA3, an  $\sim 10\%$  increase in axonal length was found in HOM and HET mice ( $P < 0.0001$ ) (Fig. S3H and J), but unlike shRNA-mediated decrease of *Disc1* (3), we did not observe any GFP-labeled axons reaching the CA2 and CA1 fields.

Notably, as with neonatally generated neurons, adult-born cells displayed deficits in the segregation of IPB and SPB, with  $\sim 20\%$  more axons crossing the pyramidal cell layer in HOM ( $P < 0.05$ ) at the expense of axons localized at the IPB ( $P < 0.05$ ) (Fig. 3E and F). Additional labeling of the entire axonal bundle of immature adult-born neurons with polysialated neural cell adhesion molecule (PS-NCAM), a marker of 1- to 3-wk-old neurons, confirmed normal targeting to the distal portions of the MF and aberrant bundling in the proximal part (Fig. S3K). Overall, our results show that *Disc1<sup>Tm1Kara</sup>* leads to a maturation-dependent decrease in dendritic complexity as well as altered axonal projections of adult-born GCs, and they do not support the notion that accelerated

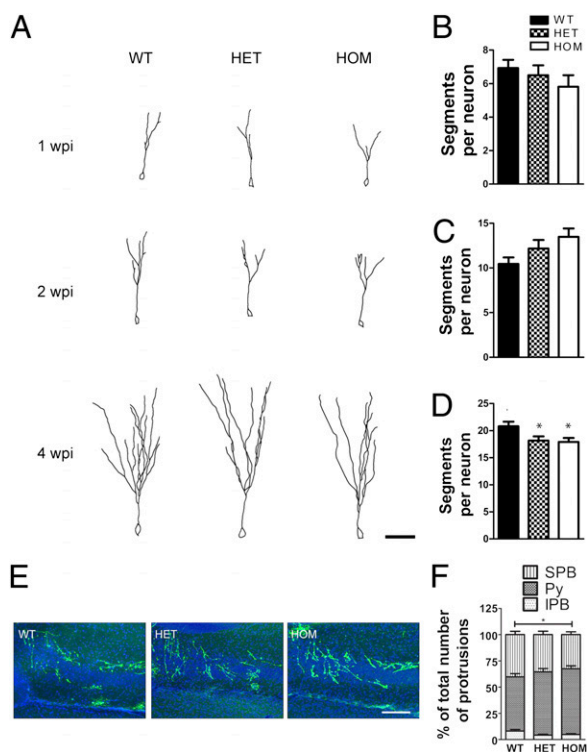


**Fig. 3.** Analysis of adult-born neurons. (A) Representative tracings of adult-born neurons at 1, 2, and 4 wpi and (B–D) quantification of the number of dendritic segments per neuron at 1 (B;  $P = 0.4$ ;  $n = 14, 18$ , and 16 cells), 2 (C;  $P = 0.319$ ;  $n = 20, 23$ , and 19 cells), and 4 wpi (D;  $P = 0.02$ ;  $n = 20, 19$ , and 22 cells). (E and F) Axonal distribution in the proximal CA3 (E). (F) More axons (in percentages) are found in the Py of HOM mice at the expense of axons located in the IPB ( $P < 0.05$ ). The difference to the SPB was not significant ( $n = 6, 6$ , and 4 mice). Values represent mean  $\pm$  SEM. \* $P < 0.05$ . (Scale bars: A, 50  $\mu\text{m}$ ; E, 100  $\mu\text{m}$ .)

maturation of adult-born neurons because of loss of function *DISC1* mutations contributes to SCHZ (23).

***Disc1*<sup>Tm1Kara</sup> Affects Short-Term Plasticity at MFT.** We tested whether changes in the axonal and dendritic architecture in *Disc1*<sup>Tm1Kara</sup> are accompanied by alterations in synaptic structure, transmission, and plasticity. Ultrastructural analysis of both pre- and postsynaptic regions in the stratum lucidum of the CA3 of adult mice using EM revealed normal gross morphology, with no overt alterations in the size of the presynaptic boutons, the size and number of dendritic spines encapsulated within, or the size and number of active zones (Fig. S4 A–G). However, although the number of vesicles in the reserve pool was unaltered, their volume was  $\sim 10\%$  smaller in mutant mice ( $P < 0.0001$ ) (Fig. 4 A–C).

MF inputs to CA3 pyramidal cells offer a unique opportunity to systematically address the effect of the *Disc1* mutations on presynaptic physiology, because they display three types of well-characterized short- and long-term presynaptic plasticity (24): (i) long term potentiation (LTP), (ii) synaptic facilitation at brief interstimulus intervals ( $\leq 200$  ms), and (iii) frequency facilitation, a form of STP unique to MFs where increased transmitter release occurs at firing frequencies as low as 0.2 Hz (25). To this end, we performed extracellular recordings of MF input to distal CA3 pyramidal neurons in stratum lucidum while stimulating the DG cell layer.

At baseline, the amplitudes of evoked field excitatory postsynaptic potentials (fEPSPs) were of comparable magnitude in WT and HOM *Disc1*<sup>Tm1Kara</sup> mice across a range of stimulus intensities (Fig. 4 D and E). To induce LTP, the GC layer was stimulated at 100 Hz for 1 s two times in the presence of aminophosphonovalerate (APV) (30  $\mu\text{M}$ ) to block NMDA receptors. A

large posttetanic potentiation (PTP; the large transient potentiation observed immediately after tetanization) was observed before fEPSPs plateaued at a sustained potentiated level, but neither PTP nor LTP was affected by *Disc1*<sup>Tm1Kara</sup> ( $P = 0.85$ ) (Fig. 4 F and Fig. S5A). To test facilitation at brief interstimulus intervals (50–200 ms), either pairs (Fig. 4 G) or four-pulse trains (Fig. S5B) of stimuli were applied to the DG. Again, there was no apparent effect of *Disc1*<sup>Tm1Kara</sup> on this parameter. However, when paired stimuli were given at intervals  $\geq 400$  ms, HOM mice displayed lower levels of facilitation than WT (Fig. 4 G). Facilitation at these longer intervals (called frequency facilitation) is thought to be mechanistically distinct from short-term facilitation (26), likely involves a chemical intermediary process (24), and can accumulate substantially during trains of action potentials. To investigate the impact of the *Disc1*<sup>Tm1Kara</sup> on frequency facilitation, the DG was stimulated 20 times at 1, 0.5, and 0.33 Hz (Fig. 4 H and I). Despite differences in facilitation when paired stimuli were given at 1-s intervals, after 20 stimuli at 1 Hz, facilitation in HOM mice was indistinguishable from WT mice. However, when the stimulation frequency was reduced, deficits became apparent that were significant at 0.33 Hz (effect of genotype:  $P = 0.03$ , genotype  $\times$  stimulus number interaction:  $P < 0.001$ ). This observation is consistent with the notion that facilitation is decaying faster in mutant mice. To test this notion, after a 1-Hz train of 20 stimuli, the stimulation frequency was decreased to 0.2 Hz to observe the decay of facilitation. Consistently, 5 s after 1 Hz-induced facilitation, the decrease in facilitation was significantly greater in mutant mice ( $P = 0.001$ ). At 0.2 Hz, recovery from facilitation was, however, incomplete, showing that, at this frequency, steady state facilitation was even more reduced in mutant mice (effect of genotype:  $P = 0.002$ , genotype  $\times$  stimulus number interaction:  $P = 0.002$ ) (Fig. 4 J). Comparing the rate at which facilitation declines with decreasing stimulation frequency showed a clear genotypic effect (Fig. 4 K). Our results show that the *Disc1* mutation adversely affects (in a frequency-dependent manner) frequency facilitation, a form of plasticity that is thought to be presynaptic in origin. The mechanistic basis of the alterations in frequency facilitation at MFT remains unknown (Discussion). Analysis of expression levels in the isolated DG (Fig. S6A) of a number of molecules that may modulate this form of plasticity [metabotropic glutamate receptor (mGluR2), kainate receptor Grik1 (GluR5) and Grik5 (KA2), ryanodine receptor, and adenylyl cyclase (AC) 8] did not reveal any changes (SI Methods and Fig. S6 B–F). Nevertheless, convergent evidence from ultrastructural and electrophysiological analysis strongly suggests that *Disc1*<sup>Tm1Kara</sup> affects presynaptic physiology. It should be noted that immunoblot analysis of synaptosomal fractions from the CA3 area revealed the presence of the major *Disc1* isoform (L) in adult WT but not HOM mice (Fig. S6G).

***Disc1*<sup>Tm1Kara</sup> Affects Excitability of GCs.** To determine if *Disc1*<sup>Tm1Kara</sup> affects the intrinsic properties of GCs and thus, their firing properties, whole-cell recordings were made from these neurons in WT and mutant mice. Neurons were selected from the outer layers of the DG and therefore, very likely represent mature developmentally derived neurons. Strikingly, the input resistance of mutant neurons was significantly lower than the input resistance of WT neurons ( $P = 0.004$ ) (Fig. 5 A). This difference occurred without a change in the average capacitance of the GCs (Fig. S5C), consistent with the observation of normal cell size in the adult mutant animals. To study how decreased input resistance affected the firing behavior of the neurons, we looked at the minimum current injection required to elicit an action potential and the firing rates of neurons in response to incrementing 500-ms current injections. Starting from resting potential (which did not differ between genotypes) (Fig. S5D), the rheobase value (100-ms square-wave current) was significantly larger for mutant neurons ( $P = 0.04$ ) (Fig. 5 B). Consistently, neurons fired fewer action potentials in response to a series of direct positive current injections (0.5 s) applied either at the resting membrane potential (Fig. 5 C) or a standardized potential of  $-80$  mV (Fig. S5E). As is

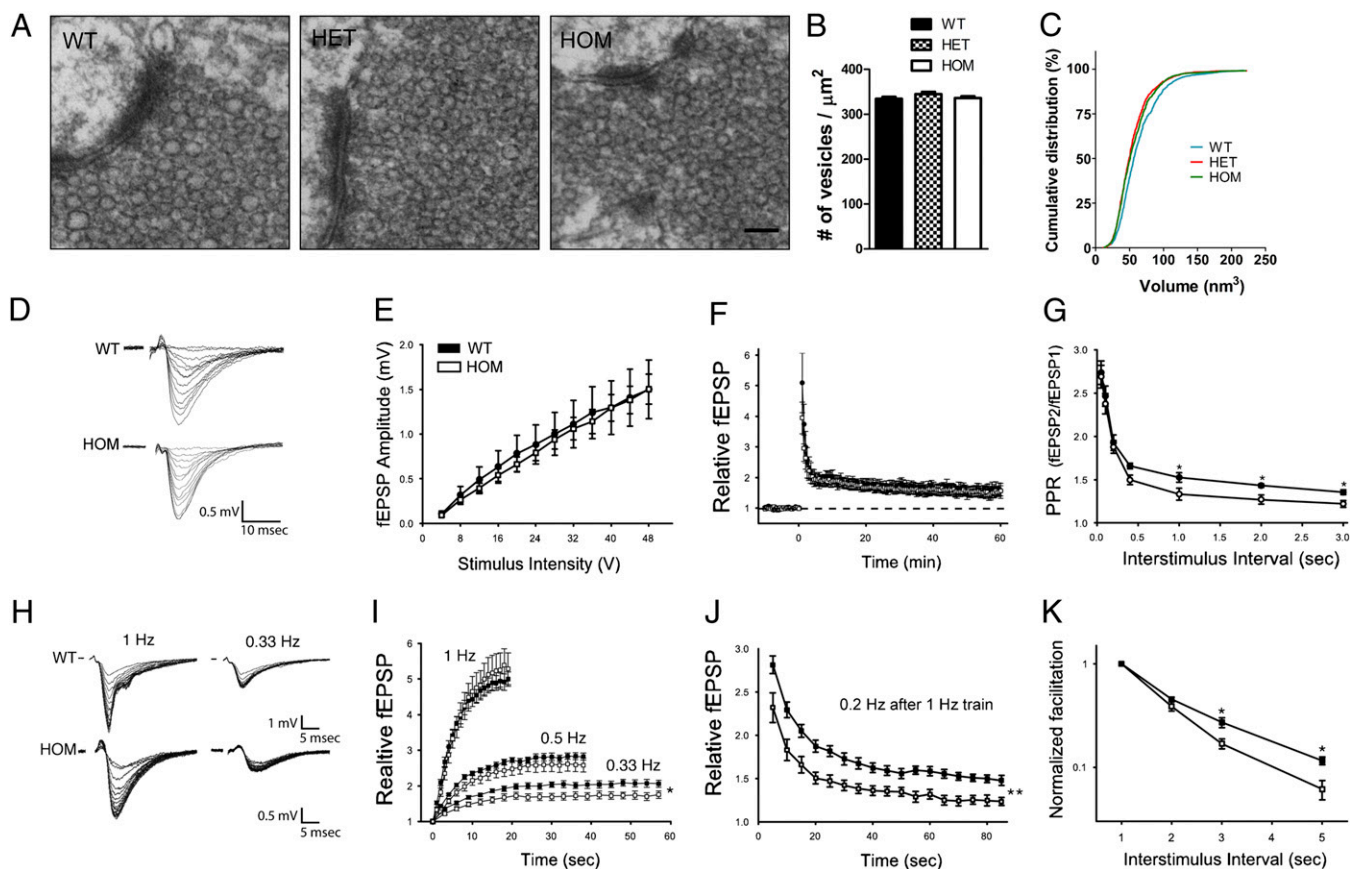


**Fig. 4.** Ultrastructural analysis and extracellular recordings of LTP and short-term plasticity at MF–CA3 synapses. (A–C) Analysis of synaptic vesicles in MFT (A) shows no change in the number of vesicles in the reserve pool (B) but a significant decrease in the volume (in micrometers cubed) of individual vesicles (C;  $P < 0.0001$ ;  $n = 1,024$  vesicles/genotype). (D) Example traces from an HOM and a WT slice over the full stimulus range. (E) The size of evoked fEPSPs was not different between genotypes over a range of stimulus intensities. (F) PTP and LTP were comparable between groups ( $P = 0.85$ ;  $n = 9$  and 8 mice). (G) Paired-pulse facilitation was tested over a wide range of interstimulus intervals (0.05–3 s); there was a significant interaction between genotype and interval, and facilitation at longer intervals (>400 ms) was reduced in HOM mice. (H) Example traces of frequency facilitation at 1 and 0.33 Hz. (I) Frequency facilitation (percent of control) in WT and HOM slices at 1 and 0.33 Hz; facilitation was significantly lower in HOM slices at 0.33 Hz (effect of genotype:  $P = 0.03$ , genotype  $\times$  stimulus number interaction:  $P < 0.001$ ;  $n = 10$  and 13 slices). (J) DG stimulation at 0.2 Hz after a train of 1-Hz stimuli (as shown in D) to assess the decay of facilitation; 5 s after the 1-Hz train, facilitation had decayed more in the HOM mice ( $67.7 \pm 3.7\%$ ) than WT mice ( $54.4 \pm 2.1\%$ ;  $P = 0.001$ ). Facilitation at 0.2-Hz stimulation then plateaus in the HOM mice at a level 58.3% lower than WT (effect of genotype:  $P = 0.002$ , genotype  $\times$  stimulus number interaction:  $P = 0.002$ ). (K) Normalizing steady state facilitation at 0.5, 0.33, and 0.2 Hz to the facilitation at 1 Hz within slices shows that facilitation decreases more rapidly in HOM slices as the frequency of stimulation is reduced. Values represent mean  $\pm$  SEM. \* $P < 0.05$ ; \*\* $P < 0.005$ . (Scale bar: A, 100 nm.)

characteristic of GC firing (27), both WT and mutant neurons displayed adaptation during the spike trains (Fig. 5D). Overall, we show that *Disc1<sup>Tm1Kara</sup>* GCs are less excitable, and this finding is likely to affect input to the CA3 region. The mechanism of altered excitability remains unknown (Discussion). Analysis of expression of Twik-1, a potassium channel implicated in the regulation of GC excitability, revealed no changes (SI Methods and Fig. S6H).

#### *Disc1<sup>Tm1Kara</sup>* Reduces PDE4 Protein Levels and Increases cAMP Levels.

Evidence from in vitro studies suggested that DISC1 may bind to and limit the activity of the cAMP-specific phosphodiesterase 4 (PDE4) (28), a family of enzymes that is critical for the degradation of cAMP, a key second messenger in the brain. However, the effect of DISC1 on PDE4 activity in vivo and most importantly, the effect of the pathogenic Scottish *DISC1* mutation on cAMP signaling remain unknown.

In contrast to the previous in vitro work that predicted an increase in PDE activity (28), analysis of PDE4 activity in the HPC of *Disc1<sup>Tm1Kara</sup>* mice revealed a robust (50%) decrease in activity in HOM mice ( $P < 0.05$ ) (Fig. 6A). Strikingly, immunoblot analysis revealed a consistent decrease in the levels of several PDE4 isoforms (Fig. 6B–I). Specifically, PDE4B1, PDE4B3, and PDE4B4 as well as PDE4D3 and PDE4D5 levels were decreased ( $P < 0.005$  and

$P < 0.05$ , respectively), whereas no difference was observed in PDE4B2 and PDE4A, indicating that *Disc1<sup>Tm1Kara</sup>* affects only selected PDE4 isoforms. This decrease was not caused by alterations in transcription, because analysis of *PDE4B* transcripts by quantitative RT-PCR (qRT-PCR) revealed no genotypic difference (Fig. S7A). Consistent with the decrease in protein levels, additional analysis revealed a pronounced decrease in the binding of rolipram, the prototypic PDE4 inhibitor, in hippocampal fractions of *Disc1<sup>Tm1Kara</sup>* mutant mice (Fig. S7B). Because in addition to PDE4 isoform levels, rolipram binding in the brain is modulated by PDE4 protein–protein interactions, this result also highlights the importance of Disc1-mediated stabilization of PDE4. In line with decreased PDE4 activity, we detected an increase in cAMP levels in hippocampal lysates ( $P < 0.05$ ) (Fig. 6J) as well as the GC layer of the DG ( $P < 0.05$ ) (Fig. 6K and L). Notably, hippocampal neurons harvested from *Disc1<sup>Tm1Kara</sup>* HOM and HET embryos and grown in culture also displayed a prominent increase in cAMP levels both at the soma (Fig. 6M and N) ( $P = 0.002$ ) and the axonal growth cone ( $P = 0.01$ ) (Fig. 6O and P), confirming a pervasive effect of Disc1 in modulating cAMP levels in mature and developing neurons.

***Disc1<sup>Tm1Kara</sup>* Affects cAMP-Dependent Pathways.** To test whether changes in PDE4 activity have an impact on cAMP-dependent

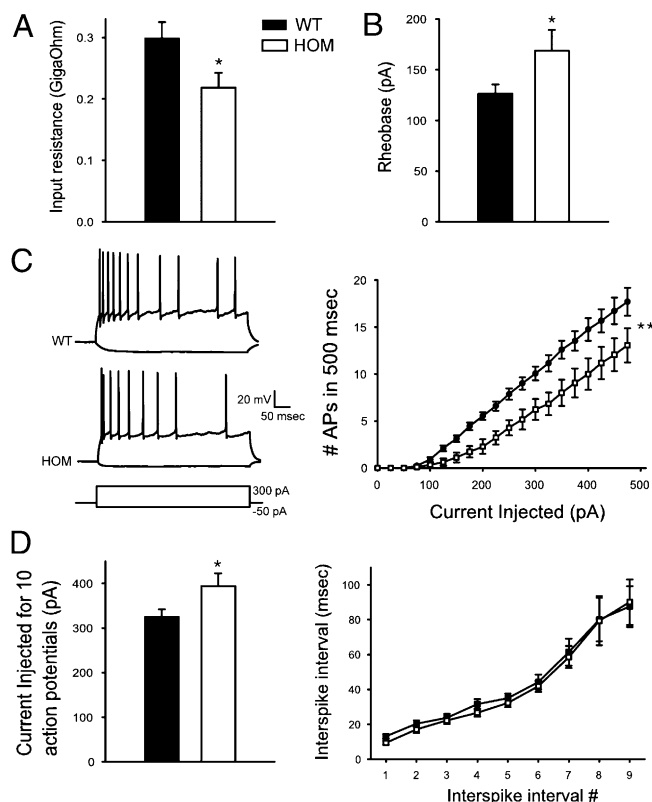


**Fig. 5.** Whole-cell recordings from GCs. (A) Input resistance of HOM GCs was 26.8% lower than input resistance of WT GCs ( $P = 0.004$ ;  $n = 15$  and 17 cells, respectively). (B) The amount of current required to evoke a single action potential (rheobase, 100-ms square-wave pulse) was 33.5% greater in HOM neurons ( $P = 0.04$ ;  $n = 6$  and 14 cells). (C *Left*) Example current-clamp recordings from WT and HOM GCs in response to hyperpolarizing ( $-50$  pA) and depolarizing ( $+300$  pA) current injections. (C *Right*) The number of action potentials evoked by 500-ms square-wave current injections (at  $+25$ -pA increments) from resting potential was lower in HOM neurons over the full range of stimulation. (D *Left*) Current injected to evoke 10 action potentials (as analyzed in D *Left*) was higher in HOM neurons ( $n = 9$  and 14 cells). (D *Right*) Adaptation during trains of 10 action potentials was not significantly different between genotypes. Values represent mean  $\pm$  SEM. \* $P < 0.05$ ; \*\* $P < 0.005$ .

pathways, we probed the phosphorylation of CREB, a downstream transcription factor activated by cAMP-dependent phosphorylation. We observed enhanced cAMP response element binding protein (CREB) phosphorylation ( $P < 0.05$ ) (Fig. 7A), raising the possibility that *Disc1<sup>Tm1Kara</sup>* results in transcriptional alterations. In other systems, elevated cAMP levels have been associated with aberrant axonal targeting through CREB-mediated transcriptional regulation of key pathfinding molecules, including those molecules belonging to neuropilin/plexin/semaphorin signaling complexes (29). The axonal lamination phenotype observed in *Disc1<sup>Tm1Kara</sup>* mutant mice and the fact that neuropilins and plexins have been extensively implicated in MF targeting, laminar-restricted positioning (30, 31), and more recently, GC dendritic outgrowth (32) prompted us to assess their levels in the DG of *Disc1<sup>Tm1Kara</sup>* mutant mice. qRT-PCR analysis on RNA from isolated DG (Fig. S64) showed a significant up-regulation of Neuropilin 1 (Nrp1) and PlexinA3 (PlxnA3), with no change in Nrp2 in adult mutant mice (Fig. 7B–D) ( $P < 0.05$ ). Immunohistochemical analysis in P11 mice also confirmed a pronounced up-regulation of the Nrp1 protein in the MF ( $P < 0.001$ ) (Fig. 7E and F) and a down-regulation of Semaphorin 3a (Sema3a), which is primarily localized in CA3 pyramidal neurons ( $P < 0.05$ ) (Fig. 7G and H). Analysis in cultured DG explants also revealed an up-regulation of Nrp1 in mutant growth cones (Fig. 7I), and treatment with a cell-perme-

able adenylyl cyclase (AC) inhibitor SQ-22536, which like all specific AC inhibitors, does not cross the blood-brain barrier but rapidly down-regulates cAMP levels in vitro (33), rescued this effect (Fig. 7J). Finally, in a complementary experiment, systemic treatment of WT mice with rolipram, an inhibitor of PDE4, resulted in up-regulation of Nrp1 in the DG (Fig. 7K and L), further supporting the role of cAMP in its expression. In summary, we showed that *Disc1<sup>Tm1Kara</sup>* results in dysregulation of molecules involved in axon guidance and dendritic growth, whose expression is modulated by cAMP signals. Notably, the pattern of dysregulation is similar to the one reported previously in the olfactory system (29).

**Altered cAMP Levels Underlie *Disc1<sup>Tm1Kara</sup>*-Linked Axonal and Dendritic Phenotypes.** The prominent increase in cAMP levels observed in the soma and growth cone of mutant hippocampal neurons afforded us the opportunity to determine whether dysregulated cAMP signaling underlies some of the axonal and dendritic phenotypes associated with *Disc1<sup>Tm1Kara</sup>*. We first determined whether these phenotypes are recapitulated in cultured neurons and then asked whether they can be reversed by manipulating cAMP levels. Neurons from *Disc1<sup>Tm1Kara</sup>* mice were first assessed for their ability to respond to repulsive cues using a stripe assay. Most WT neurites were strongly repelled from entering stripes containing the repulsive molecule ephrin-A5, whose repellent effect was previously shown to be dependent on local cAMP levels (34). By contrast, mutant neurites displayed significantly reduced repulsion ( $P < 0.05$ ) (Fig. 8A and B). Treatment with SQ-22536 increased the repulsion in HET and HOM neurons to WT levels (Fig. 8A and B). Thus, elevated cAMP levels contribute to the alterations in axonal pathfinding.

Deficits in dendritic growth were also recapitulated in hippocampal cultures. Specifically, day in vitro (DIV)5 neurons from *Disc1<sup>Tm1Kara</sup>* mice displayed a less complex dendritic tree than WT neurons (Fig. 8C–E), with decreased branch point numbers ( $P < 0.0001$ ) and total length ( $P = 0.008$ ). Expression of full-length *Disc1* normalized dendritic length and branching point numbers (Fig. 8C–E). A 25-h treatment of DIV4 neurons with SQ-22536 had no significant effect on the arborization of WT neurons; however, the decrease in dendritic complexity in HOM and HET neurons (dendritic branching:  $P < 0.005$ , dendritic length:  $P < 0.05$ ) was abolished (Fig. 8F and G), suggesting that elevated cAMP levels may contribute to the observed dendritic abnormalities.

## Discussion

This study was designed to evaluate how a bona fide pathogenic mutation that predisposes to SCHZ and other major psychiatric disorders affects the structure and function of a neural circuit at the cellular and subcellular level. Given that the DG is the site of highest *DISC1* expression in the adult brain (11) and has been implicated in SCHZ pathophysiology (12, 35), we examined the development, maturation, and excitability of dentate GCs as well as synaptic transmission and plasticity in the MF/CA3 circuit. We elucidated the impact of the pathogenic *DISC1* mutation by applying an array of morphological, neurophysiological, biochemical, and cellular assays to an etiologically valid mouse model of this mutation. This analysis led to four key findings. First, we showed that mutant GCs display aberrant axonal pathfinding, resulting in mistargeted output synapse formation. Second, we provided evidence that in the absence of full-length *Disc1* PDE signaling is impaired, resulting in elevated cAMP levels that contribute to the observed axonal pathfinding alterations. Third, we showed that mutant GCs display aberrant electrophysiological properties, including altered frequency facilitation at their synapses to pyramidal cells, which likely affects CA3 activity (36, 37). Fourth, we showed that models of pathogenic SCHZ-predisposing mutations based on germ-line engineering can affect neural circuitry in very different ways to RNAi gene-silencing approaches.

The demonstration of previously unsuspected errors in axon pathfinding that result in the ectopic localization of MFTs may have a significant impact on the transfer of information from DG

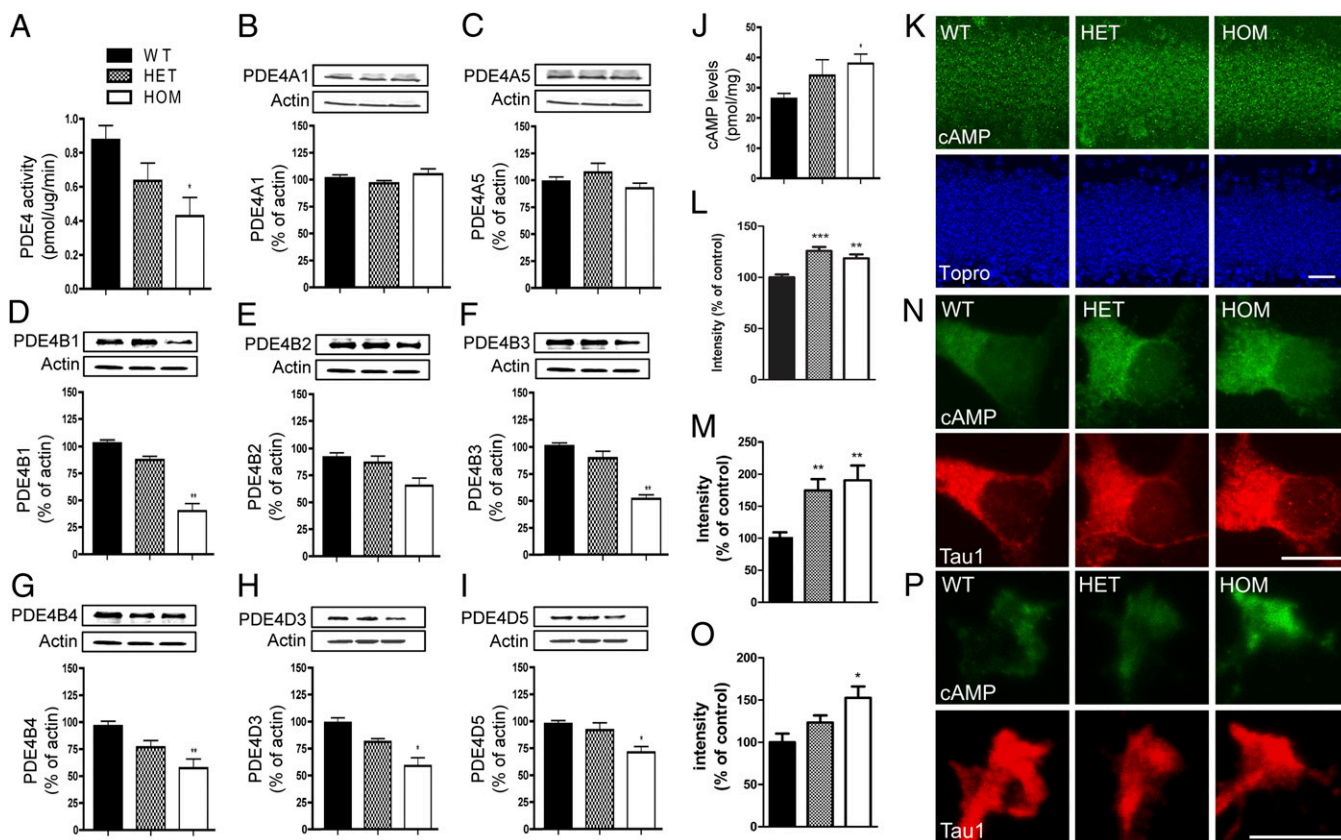


**Fig. 6.** Analysis of PDE4 and cAMP levels. (A) Decreased PDE4 activity in HOM mice (in picomoles per microgram per minute;  $P < 0.05$ ;  $n = 4$  mice/genotype). (B–I) Analysis of PDE4 isoform protein levels in the HPC of *Disc1<sup>Tm1Kara</sup>* mice showing normal levels of PDE4A splice variants (B and C), decreased PDE4B variants (D–G;  $P < 0.005$ ), and decreased PDE4D variants (H and I;  $P < 0.05$ ; expressed as percentages of WT;  $n = 4$  mice/genotype). (J–L) Increased cAMP levels in HPC lysates (J;  $P < 0.05$ ;  $n = 5$  mice/genotype) and increased cAMP immunoreactivity (as percentages of WT) in the GC layer of *Disc1<sup>Tm1Kara</sup>* mice (K and L;  $P < 0.005$ ). The GC layer is counterstained with the nuclear stain Topro (blue;  $n = 5, 6, \text{ and } 7$  mice). (M–P) Analysis of cAMP levels in hippocampal neurons. Quantification of cAMP immunoreactivity (as percentages of WT) in the cell soma (M and N;  $P = 0.002$ ;  $n = 60, 66, \text{ and } 60$  cells) and (O and P) axonal growth cones ( $P = 0.01$ ;  $n = 50, 120, \text{ and } 60$  growth cones). Cell bodies and growth cones are counterstained with Tau1. Values represent mean  $\pm$  SEM. \* $P < 0.05$ ; \*\* $P < 0.005$ ; \*\*\* $P < 0.0005$ . (Scale bars: K, 25  $\mu\text{m}$ ; N and P, 10  $\mu\text{m}$ .)

to CA3. The altered innervation of CA3 neurons is expected to affect functional connectivity, because axosomatic synapses may be more efficient than axodendritic synapses in driving discharge (38). Alterations in axonal patterning, in addition to changes in dendritic growth both early in neonatal development and in the adult brain, may cumulatively impinge on the structure and function of this neural network. Our analysis also provides a mechanistic basis for the observed axonal cytoarchitectural alterations. Specifically, we provide evidence that the pathogenic *Disc1* truncation results in decreased PDE4 protein levels and increased cAMP levels. Altered cAMP signaling, in turn, results in transcriptional dysregulation of neuronal guidance proteins and may also affect locally the behavior of the growth cones in response to external repulsive or attractive cues. These results are in line with recent findings implicating cAMP in the regulation of axonal pathfinding (29, 39) as well as dendrite formation (40) and provide strong support for altered (increased) neuronal cAMP signaling due to a bona fide SCHZ risk mutation. Notably, we have recently reported an association between SCHZ and gain of function mutations in the *VIPR2* locus (41) and showed that these mutations also enhance cAMP signaling in lymphocytes of patients.

Errors in individual axon targeting were reflected in a failure of IPB and SPB to clearly segregate into two distinct tracts. In that respect, it is interesting that earlier studies have shown distinct strain-specific patterns of MF lamination in mice, which were associated with an altered distribution of MFTs (42) and correlated with performance in cognitive tasks, including some spatial WM tasks (17, 18). There is also evidence of differential activation of

the SPBs and IPBs of the DG (43), and altered segregation of the SP and IP blades may change the respective connectivities of these blades with CA3. Although the pattern of MF lamination has not been explicitly probed in patients with SCHZ, one study has reported lower numerical density of MFTs in CA3 (44), and another study showed lighter overall staining with an MF specific marker (45) consistent with changes occurring in this pathway. More broadly, neuropathological studies have found a number of variable and modest disturbances in the overall DG-CA3 region, including reduced dendritic arborization (13, 14), implicating this region in SCHZ pathogenesis (12, 35).

In addition to altered structural connectivity, we showed that mutant GCs show changes in excitability as well as altered short-term synaptic dynamics at MF synapses, both of which have important implications for information transfer within this neural network. In particular, we showed that frequency facilitation, a form of STP at MF synapses, is adversely affected by the *Disc1* mutation. Frequency facilitation is a cumulative increase in release probability during trains of GC firing at relatively low frequencies. It is of interest that the frequencies at which aberrant frequency facilitation was detected correspond to the overall firing rates of GCs observed in vivo (0.1–1 Hz) (46, 47), suggesting that, at these basal firing rates, mutant MF synapses may be in a tonically less facilitated state. Frequency facilitation is a presynaptic process unique to MFs, and its slow temporal dynamics strongly implicate a yet unknown biochemical intermediary. Our results show that frequency facilitation decays more rapidly in mutant MFTs, suggesting that *Disc1* (either directly or indirectly) affects the per-

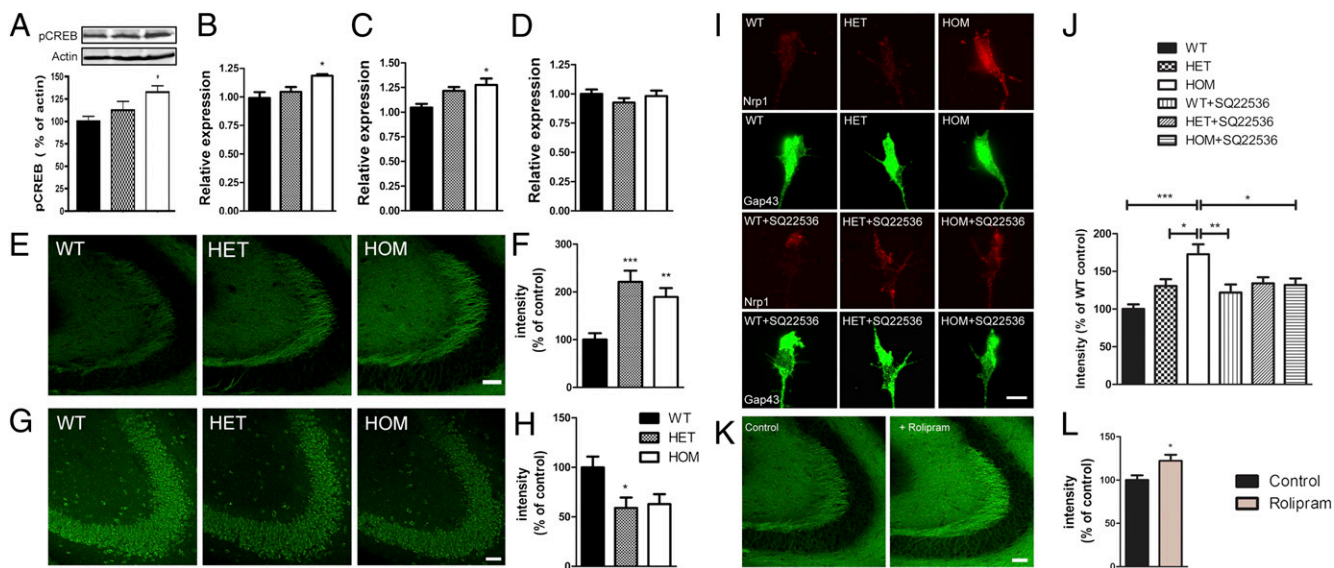


**Fig. 7.** Expression of key molecules belonging to neuropilin/plexin/semaphorin signaling complexes. (A) CREB phosphorylation is increased in the HPC of adult *Disc1<sup>Tm1Kara</sup>* mice ( $P < 0.05$ ;  $n = 5$  mice/genotype). (B–D) qRT-PCR analysis showing increased expression of *Nrp1* ( $P < 0.05$ ; B) and *Plxn3* ( $P < 0.05$ ; C) but not *Nrp2* (D) in the DG of adult mice ( $n = 8, 7,$  and  $5$  mice). (E and F) Increased *Nrp1* immunoreactivity in MFs of P11 mice (expressed as percentages of WT;  $P < 0.001$ ;  $n = 7$  mice/genotype). (G and H) Decreased *Sema3a* immunoreactivity in CA3 pyramidal neurons (expressed as percentages of WT;  $P < 0.05$ ;  $n = 7$  mice/genotype). (I and J) *Nrp1* immunoreactivity in axonal growth cones of DG explants is increased in mutant mice (I). This effect is rescued by treatment with SQ-22536 (J). Quantification (as percentages of WT;  $P < 0.005$ ;  $n = 6, 6,$  and  $5$  explants/genotype per treatment). Axons were counterstained with Gap43 (green). (K and L) *Nrp1* immunoreactivity in MF of P11 WT mice treated with rolipram (K). (L) Quantification (as percentages of control;  $P < 0.05$ ;  $n = 4$  mice/treatment). Values represent mean  $\pm$  SEM. \* $P < 0.05$ ; \*\* $P < 0.005$ ; \*\*\* $P < 0.0005$ . (Scale bars: E, G, and K, 50  $\mu$ m; I, 2  $\mu$ m.)

sistence of this facilitating signal. The signaling molecules that mediate frequency facilitation, however, remain unclear. Cases have been made for and against the involvement of presynaptic kainate receptors and intraterminal  $\text{Ca}^{2+}$  stores, but unequivocal data are lacking. Elucidating whether cAMP signaling is involved is confounded by the facts that wholesale manipulations of cAMP levels through cAMP analogs and AC activation potently and bidirectionally affect release probability and result in diverse neurophysiological outputs at MFTs (48, 49). Nevertheless, it is well-established that manipulating cAMP levels at various types of presynaptic terminals alters the dynamics of STP (50–53). Of particular interest is that chronically elevated cAMP levels can affect synaptic facilitation through effects on vesicular pools (54), and animals lacking AC8, which acts as a presynaptic calcium sensor, have WM but not long-term memory deficits (55), similar to *Disc1<sup>Tm1Kara</sup>* animals. In that respect, it is noteworthy that cyclic nucleotide-dependent vesicle recycling at presynaptic terminals and growth cones has been implicated in both synaptic plasticity (24) and axon targeting (56) and therefore, is a potential link between these processes in *Disc1<sup>Tm1Kara</sup>* animals. Along these lines, additional work needs to determine whether the volumetric change of synaptic vesicles in MFTs reflects abnormal cAMP-dependent vesicle recycling or biogenesis at the presynaptic terminal and whether it contributes to observed defects in synaptic plasticity.

In contrast to robust deficits in STP, an assay of long-term plasticity showed no effect by the mutation. That LTP is not significantly changed in mutant animals may suggest differential sensitivity of various synaptic processes to the levels of cAMP elevation or emergence of homeostatic mechanisms, which might compensate for the effect of chronically elevated cAMP on some but not all physiological properties. Similarly, the observation that GCs are less excitable in *Disc1* mutants, despite the generally pro-excitatory effects of cAMP, may indicate that reduced catabolism of cAMP, may maladaptively induce homeostatic mechanisms to reduce cell activity. Future work will investigate whether physiological changes are directly linked to increased cAMP levels or whether they are part of an adaptive/maladaptive response to the primary genetic effects.

Although our study shows that intact *Disc1* is essential for proper maturation of adult-born GCs, it did not yield data congruent with results obtained by using oncoretrovirus-mediated RNAi approaches (2–4). Previous work on the effect of *Disc1* on the DG structure and function (including on adult neurogenesis) has been based primarily on oncoretrovirus-mediated RNAi approaches (2–4). A prominent view, largely shaped by such approaches, is that *Disc1* restricts growth of adult-born neurons and that *DISC1* mutations predispose to SCHZ by releasing this constraint, resulting in robust neuronal overgrowth and misplacement as well as premature maturation (23). Although a relatively subtle mispositioning, affecting only a fraction of young GCs, has been observed in *Disc1<sup>Tm1Kara</sup>* mice (9), our findings overall do not support the notion that *DISC1* mutations increase disease risk by accelerating the normal maturation and growth of adult-born neurons. These discrepancies raise an important general issue pertaining to the information obtained by disease models based on RNAi-mediated approaches as opposed to models based on germ-line genetic lesions. Discrepant findings from such models are well-established in the literature (57, 58). Although RNAi-mediated approaches may provide information about cell-autonomous functions, they have significant limitations when used to model in vivo effects of a disease risk gene disruption. Targeting of a small portion of cells within the brain cannot reproduce the timing and magnitude of a germ-line genetic disruption and it may result in unpredictable interactions with the WT context surrounding them. Another likely explanation for some of these discrepancies is off-target effects, a well-known confounding factor of RNAi-based approaches (59, 60). Overall, our findings suggest that results from studies using RNAi techniques may need to be reevaluated in carefully designed animal models.

Our work has important implications for understanding the pathophysiology of SCHZ, especially when considered in the context of recent findings from other genetic mouse models of the disease. The pattern of widespread but modest cytoarchitectural abnormalities and altered short-term synaptic dynamics described here is similar to the one recently described in the

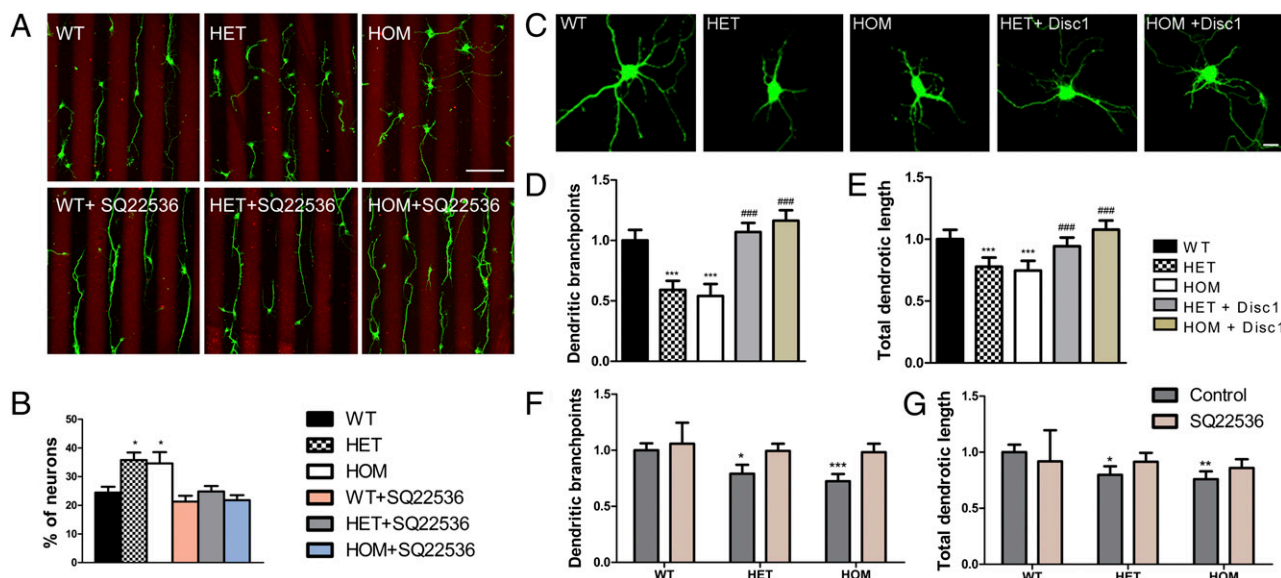


**Fig. 8.** cAMP levels and *Disc1*<sup>Tm1Kara</sup>-linked axonal and dendritic phenotypes. (A and B) Analysis of repulsive axonal guidance in vitro. (A) Hippocampal neurons were grown on alternating stripes containing ephrin-A5-Fc (red stripes) or control protein (dark stripes). (B) WT neurites were repelled on interacting with ephrin-A5, whereas mutant neurons were less sensitive; hence, more neurites crossed the ephrin-A5-containing stripes ( $P < 0.05$ ;  $n = 5, 3$ , and 3 embryos/genotype). Treatment with 10  $\mu$ M SQ-22536 increased the repulsion in HET and HOM but not WT neurons ( $n = 4, 4$ , and 7 embryos/genotype). (C) Representative images of DIV5 primary hippocampal neurons from WT, HET, and HOM embryos transfected with  $\beta$ -actin-GFP or  $\beta$ -actin-GFP and exogenous *Disc1*. (D and E) Decreased dendritic branching point numbers (D;  $P < 0.0001$ ) and total dendritic length (E;  $P = 0.008$ ; normalized to WT) of mutant DIV5 neurons transfected with  $\beta$ -actin-GFP or  $\beta$ -actin-GFP/*Disc1* ( $n = 60, 53, 51, 55$ , and 50 cells). (F and G) Rescue of impaired dendritic complexity in DIV5 neurons treated with SQ-22536. (F) Analysis of branching point numbers and dendritic length (G; dendritic branching:  $P < 0.005$ , dendritic length:  $P < 0.05$ ; control treatment:  $n = 74, 54$ , and 64 cells, SQ-22536:  $n = 64, 58$ , and 64 cells). Values represent mean  $\pm$  SEM. Asterisks (\*) denote differences among genotypes; Hash symbol (#) denotes effect of transfection on same genotypes. \* $P < 0.05$ ; \*\* $P < 0.005$ ; \*\*\* $P < 0.0005$ . (Scale bars: A, 100  $\mu$ m; C, 2  $\mu$ m.)

prefrontal cortex of mice modeling cognitive aspects of the 22q11.2 microdeletion, which is directly relevant to the high SCHZ susceptibility risk associated with this locus (61). Notably, in both cases, it was short-term and not long-term plasticity that was affected. In addition, previous exploratory analysis of CA3-CA1 synapses in *Disc1*<sup>Tm1Kara</sup> mice also provided evidence consistent with normal LTP but impaired short-term potentiation, another type of presynaptic plasticity (9). Thus, a pattern of alterations in synaptic dynamics recurs in mouse models of bona fide disease mutations, suggesting that altered modulation of synaptic behaviors over short time periods may be a general feature of SCHZ-predisposing mutations. Short-term plasticity, be it pre- or postsynaptically expressed, is critical in determining how information is transferred within and between neuronal ensembles (62, 63). Aberrations in these processes, in conjunction with errant axonal projections, could contribute to several aspects of the pathophysiology of SCHZ, including dysconnectivity, cognitive dysfunction, and impaired integration and interpretation of sensory information (64, 65).

Comparing these results to the results from a second valid genetic mouse model of SCHZ (61), we propose that altered short-term control of synaptic transmission, coupled with deficits in structural synaptic organization, represents an important neural component of the disease. The multiple short-term forms of synaptic plasticity are modulated by a variety of neurotransmitter systems and diverse cellular mechanisms (66). Their dysregulation could, therefore, be a common endpoint in neurotransmitter-based theories of SCHZ, and its complexity could also provide a neural basis for the high genetic heterogeneity of the disease (67, 68).

## Methods

**Animals.** Mutant mice were previously described (8). Analyses were performed blind to the experimental conditions and genotype using littermates produced by heterozygous matings according to the guidelines of the Columbia University Institutional Animal Care and Use Committee. All adult mice were

males (8–10 wk) except for the electrophysiology experiments, where mice were 6–8 wk for field recordings and 4–6 wk for whole-cell recordings.

**Analysis of Axonal Lamination and Axonal Terminals.** Mice were perfused with 4% paraformaldehyde, and 40- $\mu$ m vibratome coronal sections were stained with anticalbindin antibody (rabbit, 1:1,000; Swant). The distance at which the bundles separate was measured as explained in *SI Methods*. For axonal terminal analysis, 10 $\times$  images of MFs from P11 *Disc1*<sup>Tm1Kara</sup>/*Thy1*-GFP mice were scanned with the confocal microscope. For the quantification, the region of interest was defined as depicted in Fig. S2, and the number of MFT in individual areas was counted and expressed as percentage of the total MFT number. Only puncta larger than 4  $\mu$ m, most likely to represent MFT, were included in the analysis. Terminals were also evaluated using synaptophysin staining (Fig. S8).

**Electrophysiology.** Extracellular field recordings of MF-mediated synaptic events were made in transverse hippocampal slices. The recording electrode was positioned in stratum lucidum of CA3 (typically near the apex of the bend in stratum pyramidale), and the stimulating electrode was placed over the GC layer of the DG. Whole-cell recordings were made in horizontal brain slices. GCs were selected from the outer one-third of the GC layer in the DG supralimbic blade.

A description of the statistical analysis, constructs, retroviral labeling and analysis of adult-born neurons, proliferation and dendritic complexity, immunohistochemical methods, PDE4 and cAMP assays, primary cultures, stripe assays, EM analysis, and qRT-PCR can be found in *SI Methods*.

**ACKNOWLEDGMENTS.** We thank Brenda Huang and Merilee Teylan for help with the mouse colony and technical help and René Hen for his help with the retroviral injections. Stereotaxic injections were done in the Rodent Models Core of the Lieber Center for Schizophrenia Research. M. Kvajo was in part supported by an Essel Foundation National Alliance for Research on Schizophrenia and Depression Young Investigator grant, and L.J.D. was in part supported by a National Alliance for Research on Schizophrenia and Depression Young Investigator grant. A.-M.L.-B. was partially supported by Fondation pour la Recherche Médicale and Fondation Bettencourt-Schueller. This work was supported by National Institutes of Health Grants MH7068 (to M. Karayiorgou and J.A.G.), MH77235 (to J.A.G.), and MH080234 (to J.A.G.).

- Mao Y, et al. (2009) Disrupted in schizophrenia 1 regulates neuronal progenitor proliferation via modulation of GSK3beta/beta-catenin signaling. *Cell* 136:1017–1031.
- Duan X, et al. (2007) Disrupted-In-Schizophrenia 1 regulates integration of newly generated neurons in the adult brain. *Cell* 130:1146–1158.
- Faulkner RL, et al. (2008) Development of hippocampal mossy fiber synaptic outputs by new neurons in the adult brain. *Proc Natl Acad Sci USA* 105:14157–14162.
- Kim JY, et al. (2009) DISC1 regulates new neuron development in the adult brain via modulation of AKT-mTOR signaling through KIAA1212. *Neuron* 63:761–773.
- Pletnikov MV, et al. (2008) Inducible expression of mutant human DISC1 in mice is associated with brain and behavioral abnormalities reminiscent of schizophrenia. *Mol Psychiatry* 13:173–186.
- Hikida T, et al. (2007) Dominant-negative DISC1 transgenic mice display schizophrenia-associated phenotypes detected by measures translatable to humans. *Proc Natl Acad Sci USA* 104:14501–14506.
- Clapcote SJ, et al. (2007) Behavioral phenotypes of Disc1 missense mutations in mice. *Neuron* 54:387–402.
- Koike H, Arguello PA, Kvaajo M, Karayiorgou M, Gogos JA (2006) Disc1 is mutated in the 129SvEv strain and modulates working memory in mice. *Proc Natl Acad Sci USA* 103:3693–3697.
- Kvaajo M, et al. (2008) A mutation in mouse Disc1 that models a schizophrenia risk allele leads to specific alterations in neuronal architecture and cognition. *Proc Natl Acad Sci USA* 105:7076–7081.
- Nakata K, et al. (2009) DISC1 splice variants are upregulated in schizophrenia and associated with risk polymorphisms. *Proc Natl Acad Sci USA* 106:15873–15878.
- Austin CP, Ky B, Ma L, Morris JA, Shughrue PJ (2004) Expression of Disrupted-In-Schizophrenia-1, a schizophrenia-associated gene, is prominent in the mouse hippocampus throughout brain development. *Neuroscience* 124:3–10.
- Kobayashi K (2009) Targeting the hippocampal mossy fiber synapse for the treatment of psychiatric disorders. *Mol Neurobiol* 39:24–36.
- Christison GW, Casanova MF, Weinberger DR, Rawlings R, Kleinman JE (1989) A quantitative investigation of hippocampal pyramidal cell size, shape, and variability of orientation in schizophrenia. *Arch Gen Psychiatry* 46:1027–1032.
- Arnold SE, et al. (1995) Smaller neuron size in schizophrenia in hippocampal subfields that mediate cortical-hippocampal interactions. *Am J Psychiatry* 152:738–748.
- McHugh TJ, et al. (2007) Dentate gyrus NMDA receptors mediate rapid pattern separation in the hippocampal network. *Science* 317:94–99.
- Kobayashi K, Poo MM (2004) Spike train timing-dependent associative modification of hippocampal CA3 recurrent synapses by mossy fibers. *Neuron* 41:445–454.
- Crusio WE, Schwegler H (1987) Hippocampal mossy fiber distribution covaries with open-field habituation in the mouse. *Behav Brain Res* 26:153–158.
- Schwegler H, Crusio WE, Brust I (1990) Hippocampal mossy fibers and radial-maze learning in the mouse: A correlation with spatial working memory but not with non-spatial reference memory. *Neuroscience* 34:293–298.
- Niewoehner B, et al. (2007) Impaired spatial working memory but spared spatial reference memory following functional loss of NMDA receptors in the dentate gyrus. *Eur J Neurosci* 25:837–846.
- Altman J, Bayer SA (1990) Migration and distribution of two populations of hippocampal granule cell precursors during the perinatal and postnatal periods. *J Comp Neurol* 301:365–381.
- Kempermann G, Kuhn HG, Gage FH (1997) More hippocampal neurons in adult mice living in an enriched environment. *Nature* 386:493–495.
- Amaral DG, Dent JA (1981) Development of the mossy fibers of the dentate gyrus: I. A light and electron microscopic study of the mossy fibers and their expansions. *J Comp Neurol* 195:51–86.
- Dranovsky A, Hen R (2007) DISC1 puts the brakes on neurogenesis. *Cell* 130:981–983.
- Nicoll RA, Schmitz D (2005) Synaptic plasticity at hippocampal mossy fibre synapses. *Nat Rev Neurosci* 6:863–876.
- Salin PA, Scanziani M, Malenka RC, Nicoll RA (1996) Distinct short-term plasticity at two excitatory synapses in the hippocampus. *Proc Natl Acad Sci USA* 93:13304–13309.
- Gundfinger A, et al. (2007) Differential modulation of short-term synaptic dynamics by long-term potentiation at mouse hippocampal mossy fibre synapses. *J Physiol* 585:853–865.
- Staley KJ, Otis TS, Mody I (1992) Membrane properties of dentate gyrus granule cells: Comparison of sharp microelectrode and whole-cell recordings. *J Neurophysiol* 67:1346–1358.
- Millar JK, et al. (2005) DISC1 and PDE4B are interacting genetic factors in schizophrenia that regulate cAMP signaling. *Science* 310:1187–1191.
- Imai T, et al. (2009) Pre-target axon sorting establishes the neural map topography. *Science* 325:585–590.
- Cheng HJ, et al. (2001) Plexin-A3 mediates semaphorin signaling and regulates the development of hippocampal axonal projections. *Neuron* 32:249–263.
- Suto F, et al. (2007) Interactions between plexin-A2, plexin-A4, and semaphorin 6A control lamina-restricted projection of hippocampal mossy fibers. *Neuron* 53:535–547.
- Tran TS, et al. (2009) Secreted semaphorins control spine distribution and morphogenesis in the postnatal CNS. *Nature* 462:1065–1069.
- Pavan B, Biondi C, Dalpiaz A (2009) Adenylyl cyclases as innovative therapeutic goals. *Drug Discov Today* 14:982–991.
- Nicol X, et al. (2007) cAMP oscillations and retinal activity are permissive for ephrin signaling during the establishment of the retinotopic map. *Nat Neurosci* 10:340–347.
- Tamminga CA, Stan AD, Wagner AD (2010) The hippocampal formation in schizophrenia. *Am J Psychiatry* 167:1178–1193.
- Lawrence JJ, McBain CJ (2003) Interneuron diversity series: Containing the detonation—feedforward inhibition in the CA3 hippocampus. *Trends Neurosci* 26:631–640.
- Mori M, Abegg MH, Gähwiler BH, Gerber U (2004) A frequency-dependent switch from inhibition to excitation in a hippocampal unitary circuit. *Nature* 431:453–456.
- Witter MP (2007) Intrinsic and extrinsic wiring of CA3: Indications for connective heterogeneity. *Learn Mem* 14:705–713.
- Zou DJ, et al. (2007) Absence of adenylyl cyclase 3 perturbs peripheral olfactory projections in mice. *J Neurosci* 27:6675–6683.
- Shelly M, et al. (2010) Local and long-range reciprocal regulation of cAMP and cGMP in axon/dendrite formation. *Science* 327:547–552.
- Vacic V, et al. (2011) Duplications of the neuropeptide receptor gene VIPR2 confer significant risk for schizophrenia. *Nature* 471:499–503.
- Barber RP, Vaughn JE, Wimer RE, Wimer CC (1974) Genetically-associated variations in the distribution of dentate granule cell synapses upon the pyramidal cell dendrites in mouse hippocampus. *J Comp Neurol* 156:417–434.
- Chawla MK, et al. (2005) Sparse, environmentally selective expression of Arc RNA in the upper blade of the rodent fascia dentata by brief spatial experience. *Hippocampus* 15:579–586.
- Kolomeets NS, Orlovskaya DD, Uranova NA (2007) Decreased numerical density of CA3 hippocampal mossy fiber synapses in schizophrenia. *Synapse* 61:615–621.
- Goldsmith SK, Joyce JN (1995) Alterations in hippocampal mossy fiber pathway in schizophrenia and Alzheimer's disease. *Biol Psychiatry* 37:122–126.
- Jung MW, McNaughton BL (1993) Spatial selectivity of unit activity in the hippocampal granular layer. *Hippocampus* 3:165–182.
- Leutgeb JK, Leutgeb S, Moser MB, Moser EI (2007) Pattern separation in the dentate gyrus and CA3 of the hippocampus. *Science* 315:961–966.
- Kamiya H, Shinozaki H, Yamamoto C (1996) Activation of metabotropic glutamate receptor type 2/3 suppresses transmission at rat hippocampal mossy fibre synapses. *J Physiol* 493:447–455.
- Weisskopf MG, Castillo PE, Zalutsky RA, Nicoll RA (1994) Mediation of hippocampal mossy fiber long-term potentiation by cyclic AMP. *Science* 265:1878–1882.
- Kuromi H, Kidokoro Y (2000) Tetanic stimulation recruits vesicles from reserve pool via a cAMP-mediated process in Drosophila synapses. *Neuron* 27:133–143.
- Davis GW, Schuster CM, Goodman CS (1996) Genetic dissection of structural and functional components of synaptic plasticity. III. CREB is necessary for presynaptic functional plasticity. *Neuron* 17:669–679.
- Ghirardi M, et al. (1992) Roles of PKA and PKC in facilitation of evoked and spontaneous transmitter release at depressed and nondepressed synapses in Aplysia sensory neurons. *Neuron* 9:479–489.
- Castellucci VF, Nairn A, Greengard P, Schwartz JH, Kandel ER (1982) Inhibitor of adenosine 3':5'-monophosphate-dependent protein kinase blocks presynaptic facilitation in Aplysia. *J Neurosci* 2:1673–1681.
- Renden RB, Broadie K (2003) Mutation and activation of Galphas similarly alters pre- and postsynaptic mechanisms modulating neurotransmission. *J Neurophysiol* 89:2620–2638.
- Zhang M, et al. (2008) Ca-stimulated type 8 adenylyl cyclase is required for rapid acquisition of novel spatial information and for working/episodic-like memory. *J Neurosci* 28:4736–4744.
- Tojima T, Hines JH, Henley JR, Kamiguchi H (2011) Second messengers and membrane trafficking direct and organize growth cone steering. *Nat Rev Neurosci* 12:191–203.
- Govek EE, et al. (2004) The X-linked mental retardation protein oligophrenin-1 is required for dendritic spine morphogenesis. *Nat Neurosci* 7:364–372.
- Khelifaoui M, et al. (2007) Loss of X-linked mental retardation gene oligophrenin1 in mice impairs spatial memory and leads to ventricular enlargement and dendritic spine immaturity. *J Neurosci* 27:9439–9450.
- Ma Y, Creanga A, Lum L, Beachy PA (2006) Prevalence of off-target effects in Drosophila RNA interference screens. *Nature* 443:359–363.
- Schultz N, et al. (2011) Off-target effects dominate a large-scale RNAi screen for modulators of the TGF-beta pathway and reveal microRNA regulation of TGFBR2. *Silence* 2:3.
- Fénelon K, et al. (2011) Deficiency of Dgcr8, a gene disrupted by the 22q11.2 microdeletion, results in altered short-term plasticity in the prefrontal cortex. *Proc Natl Acad Sci USA* 108:4447–4452.
- Abbott LF, Regehr WG (2004) Synaptic computation. *Nature* 431:796–803.
- Mongillo G, Barak O, Tsodyks M (2008) Synaptic theory of working memory. *Science* 319:1543–1546.
- Sigurðsson T, Stark KL, Karayiorgou M, Gogos JA, Gordon JA (2010) Impaired hippocampal-prefrontal synchrony in a genetic mouse model of schizophrenia. *Nature* 464:763–767.
- Fletcher PC, Frith CD (2009) Perceiving is believing: A Bayesian approach to explaining the positive symptoms of schizophrenia. *Nat Rev Neurosci* 10:48–58.
- Xu-Friedman MA, Regehr WG (2004) Structural contributions to short-term synaptic plasticity. *Physiol Rev* 84:69–85.
- Xu B, et al. (2008) Strong association of de novo copy number mutations with sporadic schizophrenia. *Nat Genet* 40:880–885.
- Xu B, et al. (2009) Elucidating the genetic architecture of familial schizophrenia using rare copy number variant and linkage scans. *Proc Natl Acad Sci USA* 106:16746–16751.